671

Effect of carbon-supported and unsupported Pt–Ru anodes on the performance of solid-polymer-electrolyte direct methanol fuel cells

A.S. ARICÒ[1]*, A.K. SHUKLA[2], K.M. EL-KHATIB[1,3], P. CRETÌ and V. ANTONUCCI[1]

[1]*Institute CNR-TAE, via Salita S. Lucia Sopra Contesse 39, 98126 S. Lucia, Messina, Italy;*
[2]*Solid State and Structural Chemistry Unit, Indian Institute of Science, Bangalore-560012, India;*
[3]*On leave from the Chemical Engineering and Pilot-Plant Department, National Research Center, Dokki, Giza, Egypt*
(*author for correspondence, e-mail: arico@itae.me.cnr.it; fax: +39 90 624247)*

Abstract

The structure, chemistry and morphology of commercially available carbon-supported and unsupported Pt–Ru catalysts are investigated by X-ray diffraction, energy-dispersive analysis by X-rays and electron microscopy. The catalytic activities of these materials towards electrooxidation of methanol in solid-polymer-electrolyte direct methanol fuel cells have been investigated at 90 °C and 130 °C with varying amounts of Nafion® ionomer in the catalytic layer. The unsupported Pt–Ru catalyst exhibits higher performance with lower activation-control and mass-polarization losses in relation to the carbon-supported catalyst.

1. Introduction

Solid-polymer-electrolyte direct methanol fuel cells (SPE–DMFCs) are being projected as potential electrochemical power sources for vehicular traction from the point of view of simplicity of design and hence of cost [1–5]. A SPE–DMFC comprises a membrane electrolyte coated on one side with platinum which constitutes the cathode and the other side with platinum–ruthenium that forms the anode. In the literature, although most of the studies on SPE–DMFCs have employed carbon-supported Pt–Ru anodes [6–10], recent investigations with unsupported Pt–Ru anodes have demonstrated substantially higher cell performance in relation to those utilising carbon-supported Pt–Ru anodes [11–13]. Whilst the power densities (0.2–0.35 W cm^{-2}) for SPE–DMFCs achieved from these studies are sufficient to suggest that stack construction is well worthwhile, efforts are continuously being made to enhance the performance of SPE–DMFCs in terms of cell efficiency which under operation at 80 °C with 1 M methanol and air happens to be 40–45%. In this context, it would be mandatory to realise higher Pt–Ru catalyst activities, and, for this purpose, it would be seminal to have an understanding on the morphologies of both the carbon-supported and unsupported Pt–Ru anode catalysts as well as their influence on the performance of SPE–DMFCs. In the past, morphological data have been utilised effectively in optimising the performance of the fuel cell electrodes [14–16]. As part of our on-going research [17, 18], this communication reports a study on the morphologies of both the carbon-supported and unsupported Pt–Ru anodes, and their effect on the performance of SPE–DMFCs.

2. Experimental details

Both carbon-supported (60% Pt–Ru 1:1 Vulcan–XC) and unsupported (Pt–RuO$_x$ 1:1) Pt–Ru catalysts employed during this study were obtained from E-Tek Inc., USA. Powder X-ray diffraction (XRD) patterns for these catalysts were obtained on a Philips X-Pert 3710 X-ray diffractometer using CuK$_\alpha$-source operating at 40 kV and 30 mA. All the XRD patterns were recorded at a scan rate of 0.5° 2θ min^{-1}, and were analysed by using related JCPDS files. The peak profiles of the (2 2 0) reflection in the XRD patterns of the respective catalysts were obtained by Marquardt algorithm. Instrumental broadening was determined against a

standard platinum sample under identical experimental conditions. Transmission electron-micrographs for the catalyst samples were obtained using a Philips-C12 transmission electron microscope with spatial resolution of 0.2 nm. To obtain the electron micrographs the catalyst samples were finely grinded and ultrasonically dispersed in isopropyl alcohol. A drop of the resultant dispersion was deposited and dried on to a standard copper-grid coated with carbon. The energy dispersive analysis by X-rays (EDAX) on the catalyst samples was carried out on a Philips XL-20 scanning electron microscope equipped with LaB_6-filament and operating at an acceleration voltage of 20 kV.

To prepare the membrane electrode assemblies (MEAs), a thin diffusion-layer comprising acetylene black and 20 wt % Teflon was first pasted on to a carbon cloth followed by the catalyst layer consisting of the catalyst with 15 or 33 wt % Nafion®. Both the anode and cathode were prepared in this manner and hot-bonded on either side of a pretreated Nafion®-112 membrane at 130 °C. During the study, the constitution of the cathode in all the MEAs was kept identical. Also, the catalyst loading at the cathodes and anodes in all the MEAs was maintained close to 2 mg cm^{-2}. The SPE–DMFC was assembled by mounting the MEA into a Globe-Tech cell where the anode and cathode contacts are made on their rears with serpentine flow-pattern machined from a high density graphite. Aqueous methanol (1 M) was vaporized in a preheater kept at 140 °C before being fed to the anode chamber of SPE–DMFC through a peristaltic pump; the temperature at the inlet of the cell was close to 100 °C; humidified oxygen or air preheated at 100 °C was circulated through the cathode chamber. Pressures in the anode and cathode compartments were fixed at 2 and 3 atm, respectively, through back-pressure regulators. Galvanostatic polarization data on the SPE–DMFC were collected at various temperatures under steady-state conditions. The active geometrical area of the cell was 5 cm^2. The cell resistance was determined during the polarization studies by the current-interrupter method.

3. Results and discussion

The XRD patterns for the carbon-supported and unsupported Pt–Ru catalysts employed during this study are shown in Figures 1(a) and (b), respectively. We find a distinct shift to lower Bragg angles in the XRD pattern for the unsupported Pt–Ru catalyst in relation to the carbon-supported Pt–Ru catalyst. This suggests that the degree of alloying of Pt with Ru in the unsupported Pt–Ru catalyst is lesser than in carbon-

supported Pt–Ru catalyst. To further examine the other components present in the unsupported Pt–Ru catalyst, we have attempted to resolve its XRD pattern between the 2θ-scan range from 20° to 52° as shown in Figure 2. We find the distinct presence of RuO_2 in the catalyst which is absent in the carbon-supported Pt–Ru sample. Both the catalyst samples were also subjected to energy dispersive analysis by X-rays (EDAX). While carbon-supported Pt–Ru catalyst has a well defined Pt–Ru alloy phase present in it, from the lattice parameter of the Pt–Ru f.c.c.-structure and EDAX data (Figure 3), it is found that the unsupported Pt–Ru catalyst has 50% of Ru present as an alloy with Pt and a similar amount present as oxidized ruthenium (RuO_2). We have also estimated the average size of the Pt–Ru particles in both
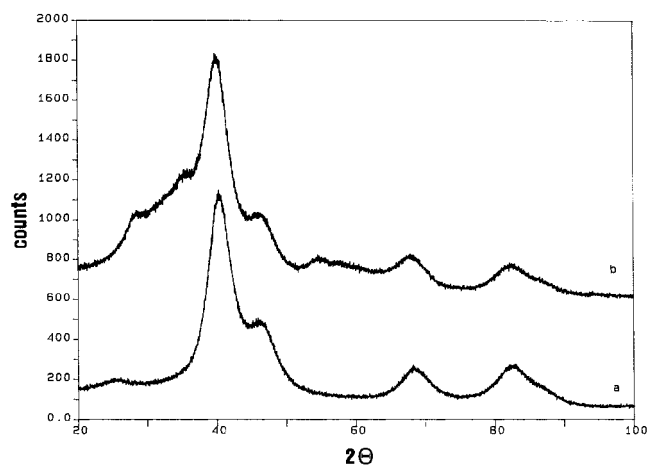

Fig. 1. XRD patterns of (a – upper line) carbon-supported Pt–Ru and (b – lower line) unsupported Pt–Ru catalysts.
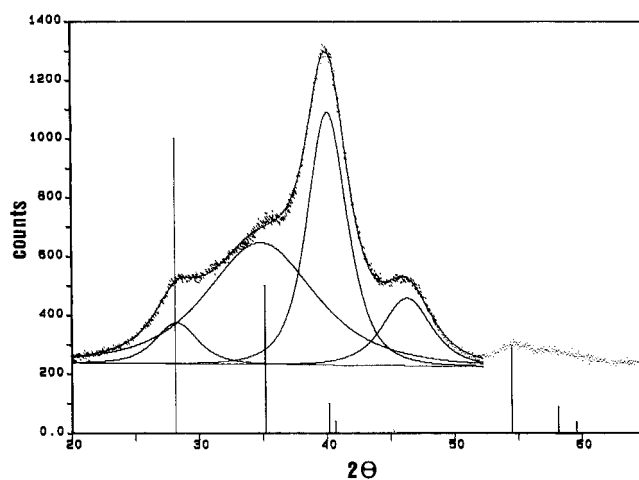

Fig. 2. Deconvoluted XRD pattern for the unsupported Pt–Ru catalyst. The lines indicate the RuO_2 phase.
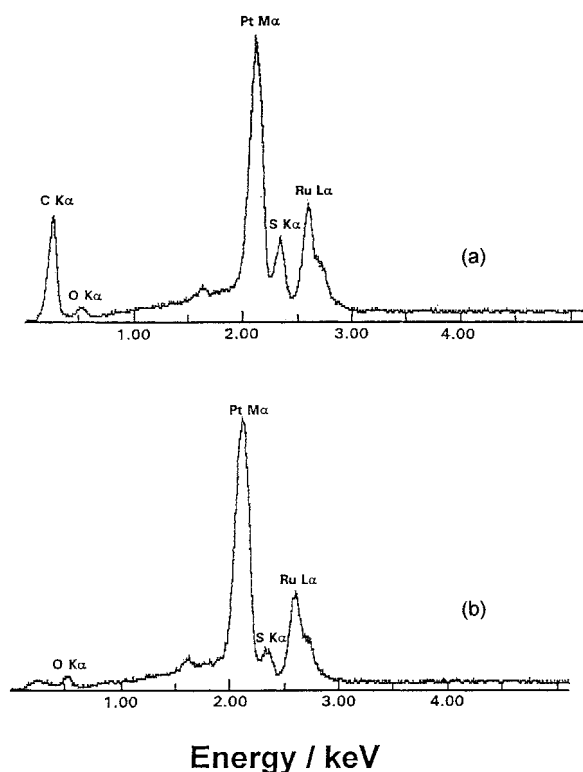
Fig. 3. EDAX data for (a) carbon-supported Pt–Ru and (b) unsupported Pt–Ru catalysts.

Fig. 4. Electron micrograph for the carbon-supported Pt–Ru catalyst.

these catalyst samples from the broadening of (2 2 0) reflection peak of their f.c.c.-structure and the Debye–Scherrer equation, and have found it to be 23 Å and 21 Å for the carbon-supported and unsupported Pt–Ru catalysts, respectively. To further elucidate on the morphologies of these catalysts, their electron micrographs have also been obtained as shown in Figures 4 and 5. A homogeneous dispersion is observed in the carbon-supported Pt–Ru catalyst with an average particle-size of 20 Å which is close to the value of 23 Å obtained from its XRD data; a few catalyst-free carbon particles of about 300 Å are also seen in this catalyst (Figure 4). On the other hand, the electron micrograph for the unsupported Pt–Ru catalyst (Figure 5) shows the presence of particle agglomerates with different contrast suggesting the presence of both Pt–Ru alloy and RuO_2 phases. Although the estimation of particle sizes in the unsupported catalyst is unwieldy, a reasonable agreement is seen with the values derived from its X-ray data.

The galvanostatic polarization data obtained at 90 °C and 130 °C for the SPE–DMFC assembled with the MEA employing carbon-supported Pt–Ru anode catalyst and 15 wt % Nafion® in its catalyst layer, and operating with 1 M aqueous methanol fuel and oxygen (SPE–DMFC 1) are shown in Figure 6; the respective
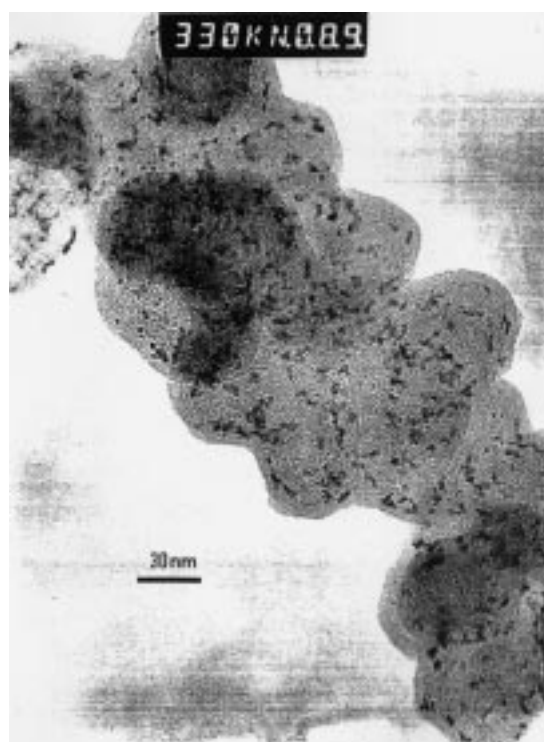

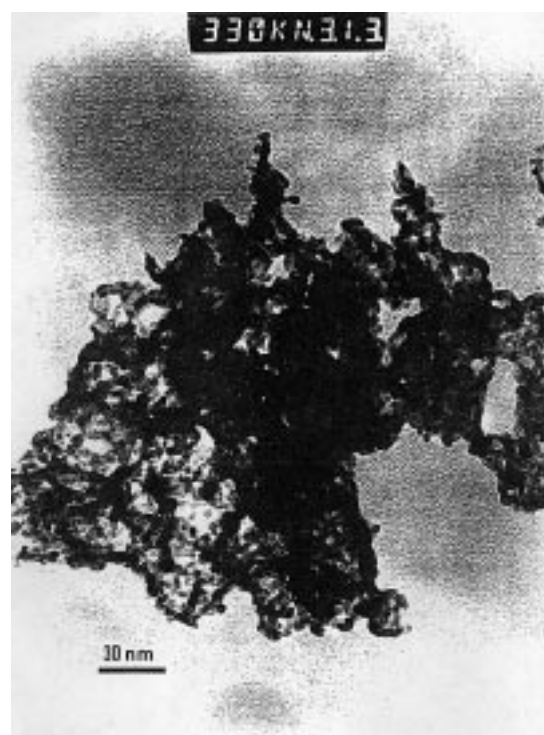Fig. 5. Electron micrograph for the unsupported Pt–Ru catalyst.

674

Fig. 6. Galvanostatic polarization data for SPE–DMFC 1. Key: (○) 90 °C; (▼) 90 °C iR-free; (▲) 130 °C; (◆) 130 °C iR-free.

Fig. 7. Galvanostatic polarization data for SPE–DMFC 2. Key: (○) 90 °C; (▼) 90 °C iR-free; (▲) 130 °C; (◆) 130 °C iR-free.
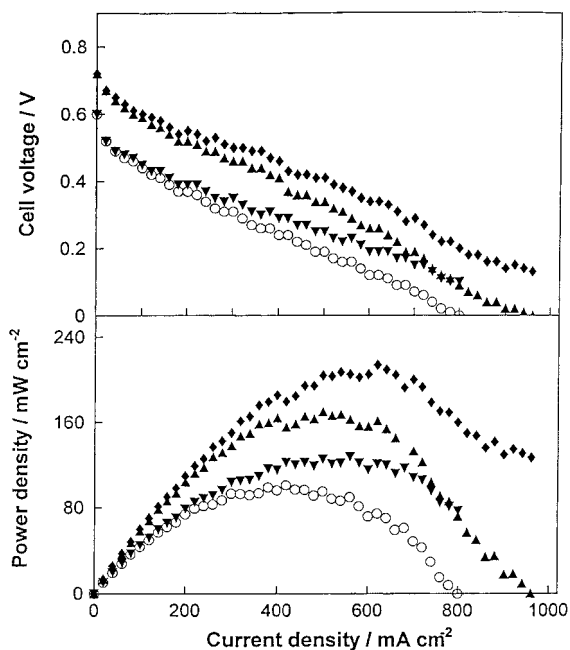

Fig. 8. Galvanostatic polarization data for SPE–DMFC 3. Key: (○) 90 °C; (▼) 90 °C iR-free; (▲) 130 °C; (◆) 130 °C iR-free.

data for the SPE–DMFC assembled with the MEA employing carbon-supported catalyst with 33 wt % Nafion® in the catalyst layer (SPE–DMFC 2) are shown in Figure 7. The performance of the SPE–DMFC 2 is only marginally superior to the performance of SPE–DMFC 1. The SPE–DMFC 2 gave a maximum power output of about 200 mW cm^{-2} at 130 °C as compared to the value of about 170 mW cm^{-2} for SPE–DMFC 1.

The galvanostatic polarization data obtained at 90 °C and 130 °C for the SPE–DMFC assembled with the MEA employing unsupported Pt–Ru anode catalyst and 15 wt % Nafion® in the catalyst layer, and operating with 1 M aqueous methanol fuel and oxygen (SPE–DMFC 3) are shown in Figure 8. The respective data for the SPE–DMFC assembled with MEA employing un-supported Pt–Ru anode and 33 wt % Nafion® in the catalyst layer (SPE–DMFC 4) are shown in Figure 9. In contrast to the data in Figures 6 and 7, the performance of the SPE–DMFC 3 having lower Nafion® loading is superior to that of the SPE–DMFC 4. While a maxi-mum power output of about 260 mW cm^{-2} at 130 °C is attained with the SPE–DMFC 3, it is only about 220 mW cm^{-2} for the SPE–DMFC 4. The polarization data obtained at 90 °C and 130 °C for the SPE–DMFC assembled with MEA employing unsupported Pt–Ru anode with 15 wt % Nafion® in the catalyst layer, and operating with 1 M aqueous methanol fuel and air (SPE–DMFC 5) are shown in Figure 10. It has been
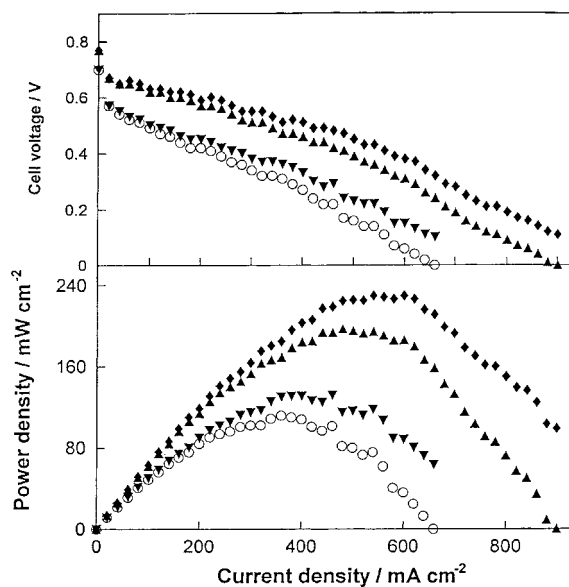
possible to attain a maximum power output of only about 180 mW cm^{-2} while using air as cathode feed at 130 °C with SPE–DMFC 5 under these operating conditions. As seen from Figures 6–9, when employing pure oxygen, the SPE–DMFC shows a marked increase

Fig. 9. Galvanostatic polarization data for SPE–DMFC 4. Key: (○) 90 °C; (▼) 90 °C iR-free; (▲) 130 °C; (◆) 130 °C iR-free.
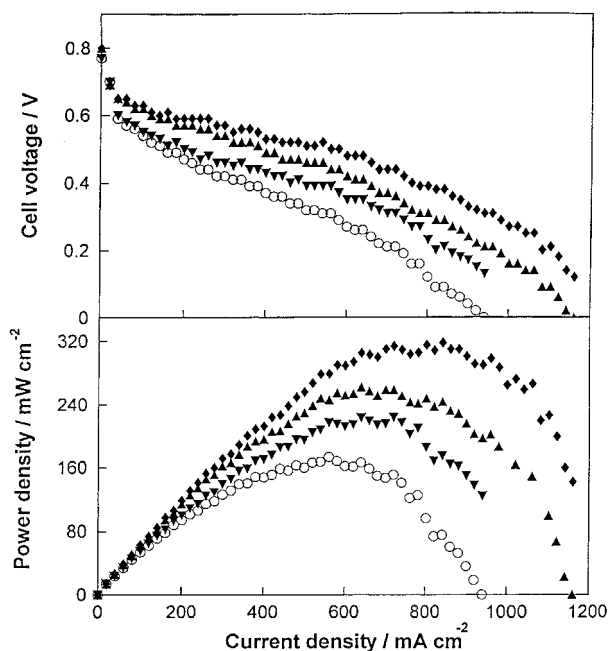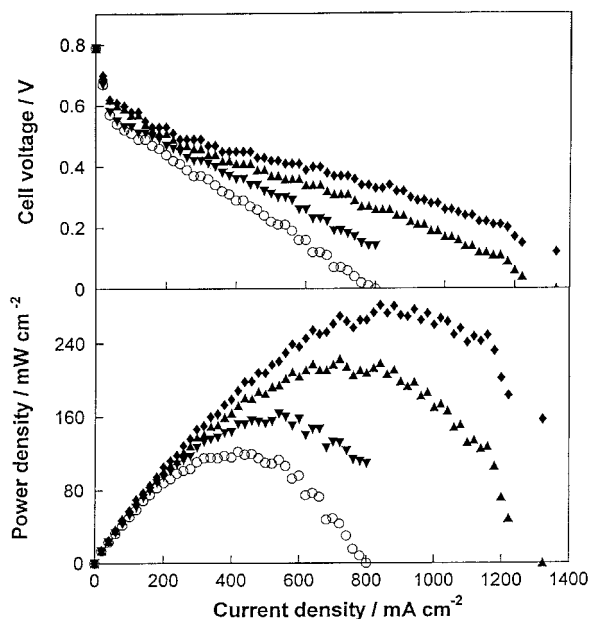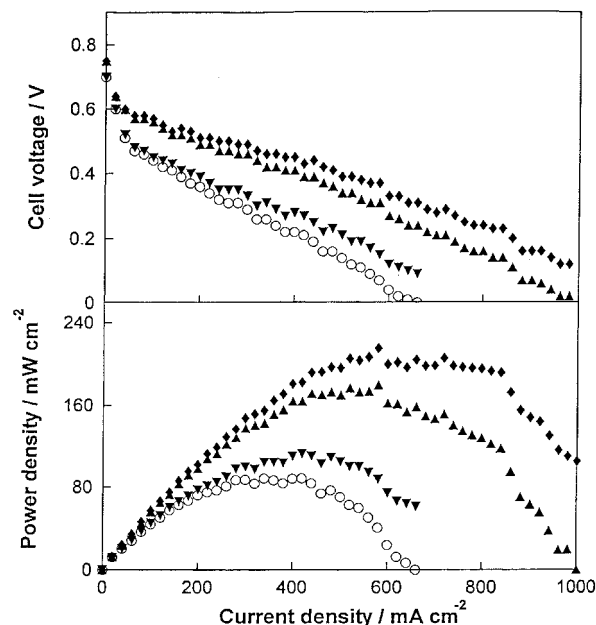

Fig. 10. Galvanostatic polarisation data for SPE–DMFC 5. Key: (○) 90 °C; (▼) 90 °C iR-free; (▲) 130 °C; (◆) 130 °C iR-free.

in performance as its temperature is raised from 90 °C to 130 °C. The internal resistance of the cell decreased from 0.14 to 0.08 Ω cm^{-2} as the temperature varied between 90 °C and 130 °C. The increase of performance with temperature may be attributed to both reduction of ohmic resistance and increase in the rate of methanol oxidation at the anode [11]. A proportional improvement in performance of SPE–DMFC 5 on increasing its temperature while using air as cathode feed is also observed (Figure 10). The lower power densities observed with SPE–DMFC 5 at both temperatures is attributed to two effects. A higher cathode poisoning due to methanol cross-over in presence of lower O_2

partial pressure severely inhibits the platinum catalyst for oxygen reduction. Oxygen transport towards active catalytic sites is hindered by the accumulation of nitrogen molecules which act as a diffusion barrier. The specific activities and cell voltages of various SPE–DMFCs at maximum power outputs are given in Table 1. Among the configurations studied, SPE–DMFC 3 shows the best performance (Table 2). At 0.5 V of the operating cell voltage, the carbon-supported catalyst shows superior performance with 33 wt % Nafion® in the catalyst layer with respect to that with 15 wt % Nafion®. However, an opposite effect is seen with the unsupported Pt–Ru catalyst. It is hypothesised that in

Table 1. Specific activities and cell voltages for different SPE–DMFCs at the maximum power outputs

	SPE–DMFC 1	SPE–DMFC 2	SPE–DMFC 3	SPE–DMFC 4	SPE–DMFC 5
Catalyst type	Carbon-supported	Carbon-supported	Unsupported	Unsupported	Unsupported
Catalyst-layer Nafion® loading/wt %	15	33	15	33	15
Maximum power Output/mW cm^{-2}	170	197	262	223	180
Specific activity/A g^{-1}	250	240	320	360	290
Cell voltage/V	0.41	0.41	0.41	0.31	0.31

Table 2. Load current densities (mA cm^{-2}) of the SPE–DMFCs at operational cell-voltage of 0.5 V

SPE–DMFC 1		SPE–DMFC 2		SPE–DMFC 3		SPE–DMFC 4		SPE–DMFC 5	
90 °C	130 °C	90 °C	130 °C	90 °C	130 °C	90 °C	130 °C	90 °C	130 °C
40	240	100	340	160	400	140	220	40	200

the carbon-supported Pt–Ru catalyst nearly half of the Nafion® ionomer is in direct contact with carbon and hence a higher loading of Nafion® in the catalytic layer, as compared to the unsupported catalyst, would be desirable to establish an optimum interface between the Nafion® micelles and Pt–Ru sites.

From the above observations, it is clear that the key step in the preparation of MEAs requires the formation of a catalyst-membrane interface which provides a large electrochemically active surface in conjunction with high H^+-ion conductivity. The preparation of such MEAs involves the formation of composite electrode-layers comprising the catalyst and proton-conducting material, namely Nafion®, and hot-bonding of these layers to the proton-conducting membrane, namely Nafion®-112. Considerable differences in the performance of the SPE–DMFCs could arise from the methods employed for preparing the MEAs. For instance, altogether different situations arise when the catalyst layer is prepared from carbon-supported and unsupported Pt–Ru anode catalysts. For preparing the carbon-supported catalyst, a large surface-area carbon, namely Vulcan XC-72, is employed as the support. Such a large surface area carbon will easily accommodate a high amount of catalyst with fine dispersions, but the presence of the micropores will obstruct the homogeneous distribution of the catalyst on to the carbon support. This in turn will hinder the mass transport in the catalyst layer by masking the access of the reacting species to the inner catalyst sites. By contrast, the unsupported catalyst, by very virtue of its preparation method, will distribute itself homogeneously in the catalyst layer and facilitate the reacting species migration in the catalyst layer in relation to the catalyst layer formed with carbon-supported Pt–Ru catalyst and Nafion®. In the light of the above discussion, we expect the performance of the SPE–DMFCs employing unsupported catalyst and Nafion® in the catalyst layer of the MEAs to be superior to those having carbon-supported catalyst and Nafion® in the catalyst layer of the MEAs. Some influence could also be observed due to the presence of an oxidized phase in the unsupported Pt–Ru catalyst. However, a previous study on the influence of RuO_2 species for the methanol electrooxidation has suggested little effect [19]. Accordingly, the observed differences in the performance of the carbon-supported and unsupported Pt–Ru catalysts studied here are mainly attributed to their morphologies.

4. Conclusion

The study suggests that it is important to optimise the morphology of the catalyst layer in the MEAs for the SPE–DMFCs. It is found that a superior performance of the SPE–DMFCs is achieved with the catalyst layer comprising unsupported Pt–Ru anode catalyst and 15 wt % Nafion®. It is argued that the unsupported Pt–Ru catalyst with Nafion® forms a homogeneously distributed composite in the catalyst layer.

References

1. K. Kordesch and G. Simader, 'Fuel Cells and their Applications' (VCH, Weinheim, 1996).
2. A. Hamnett, Phil. Trans. R. Soc. Lond. A354 (1996) 1653.
3. M.P. Hogarth and G.A. Hards, Platinum Metal Rev. 40 (1996) 150.
4. C. Lamy and J-M. Léger, Proc. Second international symposium on 'New materials for fuel cells and modern battery systems', edited by O. Savadogo and P.R. Roberge (Montrèal, Canada, 1997), pp. 477–87.
5. A.K. Shukla, M.K. Ravikumar and K.S. Gandhi, J. Solid State Electrochem. 2 (1998) 117.
6. A.K. Shukla, P.A. Christensen, A. Hamnett and M.P. Hogarth, J. Power Sources 55 (1995) 87.
7. M.K. Ravikumar and A.K. Shukla, J. Electrochem. Soc. 143 (1996) 2601.
8. A.S. Aricò, P. Creti, H. Kim, R. Mantegna, N. Giordano and V. Antonucci, J. Electrochem. Soc. 143 (1996) 3950.
9. A.S. Aricò, P. Creti, P.L. Antonucci and V. Antonucci, Electrochem. Solid State Lett. 1 (1998) 4.
10. D.H. Jung, C.H. Lee, C.S. Kim and D.R. Shin, J. Power Sources 71 (1998) 169.
11. X. Ren, M.S. Wilson and S. Gottesfeld, J. Electrochem. Soc. 143 (1996) L12.
12. S.R. Narayanan, W. Chun, T.I. Valdez, B. Jeffries-Nakamura, H. Frank, S. Surampudi, G. Halpert, J. Kosek, C. Cropley, A.B. LaConti, M. Smart, Q. Wang, G. Surya Prakash and G.A. Olah, Program and Abstracts, Fuel Cell Seminar (1996), pp. 525–8.
13. M. Baldauf and W. Preidel, Symposium on 'Electrochemical Energy Conversion and Storage for Mobile Applications' (Ulm, Germany, 1998).
14. K.V. Ramesh, P.R. Sarode, S. Vasudevan and A.K.Shukla, J. Electroanal. Chem. 223 (1987) 91.
15. A.K. Shukla, K.V. Ramesh, R. Manoharan, P.R. Sarode and S. Vasudevan, Ber. Bunsenges. Phys. Chem. 89 (1985) 1261.
16. A.K. Shukla, M.K. Ravikumar, A. Roy, S.R. Barman, D.D. Sarma, A.S. Aricò, V. Antonucci, L. Pino and N. Giordano, J. Electrochem. Soc. 141 (1994) 1517.
17. A.S. Aricò, P. Creti, Z. Poltarweski, R. Mantegna, H. Kim, N. Giordano and V. Antonucci, Mater. Chem. Phys. 47 (1997) 257.
18. A.S. Aricò, P. Creti, P.L. Antonucci, J. Cho, H. Kim and V. Antonucci, Electrochim. Acta. 43 (1998) 3719.
19. A.N. Buckley and B.J. Kennedy, J. Electroanal. Chem. 302 (1991) 261.